CARBON 81 (2015) 505–513

Available at www.sciencedirect.com

ScienceDirect

journal homepage: www.elsevier.com/locate/carbon

Elastomeric behavior of exfoliated graphite, as shown by instrumented indentation testing

Po-Hsiu Chen, D.D.L. Chung *

Composite Materials Research Laboratory, University at Buffalo, State University of New York, Buffalo, NY 14260-4400, United States

ARTICLE INFO

Article history:
Received 25 July 2014
Accepted 28 September 2014
Available online 6 October 2014

ABSTRACT

This paper reports for the first time the elastomeric behavior of a non-polymeric material, as observed in exfoliated graphite compacts (⩽12 vol.% solid, preferably 4 vol.% solid) and enabled by the high-amplitude reversible and easy sliding of the graphite layers within the cell wall of exfoliated graphite. The reversibility is probably due to the cellular structure of exfoliated graphite. The elastomeric character is independent of the maximum load and essentially unchanged upon reloading. The total and reversible engineering shear strains of the cell wall (~60 graphite layers, ~20 nm thick) are up to 40 and 35 respectively during instrumented indentation (in the compaction direction) without fracture of the layers, compared to corresponding values of 12 and 8 for flexible graphite (38 vol.% solid). The fraction of displacement that is irreversible is as low as 12%, compared to 29% for flexible graphite. The modulus is as low as 83 kPa, compared to 790 kPa for flexible graphite. The greater the degree of compaction, the lower are the shear strain and reversibility, and the higher are the modulus and the displacement load. The ease of interlayer sliding is inadequate in flexible graphite or highly-oriented pyrolytic graphite (prior work) for substantial elastomeric behavior.

1. Introduction

Exfoliated graphite is expanded graphite obtained by the exfoliation of intercalated graphite [1–3]. The intercalate (e.g., nitric acid) is a foreign species that resides (typically as monolayers) between some of the graphite layers. The exfoliation process typically involves rapid heating and is driven by the tendency for the intercalate in the graphite to vaporize or decompose upon heating. The expansion occurs along the c-axis of the graphite and can be by hundreds of times. After exfoliation, a graphite flake becomes long along the c-axis and exhibits a cellular structure, so that it looks like a worm and is referred to as a worm. The cellular structure stems from the existence of intercalate islands in the intercalated graphite. The islands are according to the Daumas-Herold Model of the structure of intercalated graphite [4]. During exfoliation, an intercalate island expands like a balloon and becomes a cell in the cellular structure [5]. The ballooning is enabled by the extensive sliding between the graphite layers in the cell wall, which consists of multiple graphite layers (e.g., about 60 layers [6]). In other words, the sliding allows the balloon wall to stretch extensively.

Due to the cellular structure, the compression of a collection of worms in the absence of a binder results in mechanical interlocking among the worms. As a consequence of the interlocking, a flexible sheet known as “flexible graphite” is

* *Corresponding author:* Fax: +1 (716) 645 2883.
E-mail address: ddlchung@buffalo.edu (D.D.L. Chung).
URL: http://alum.mit.edu/www/ddlchung (D.D.L. Chung).
http://dx.doi.org/10.1016/j.carbon.2014.09.083
0008-6223/

formed [7,8]. The sheet exhibits preferred orientation of the graphite layers in the plane of the sheet, as shown by the anisotropy in both electrical and thermal conductivities [9]. Due to the preferred orientation and the cellular structure, the sheet is resilient in the direction perpendicular to the sheet. This resiliency contributes to the ability of flexible graphite to serve as a gasket, such as a gasket for sealing fluids [8,10]. Because graphite is chemically and thermally resistant, the gasket is particularly valuable for functioning under harsh environments. In addition, flexible graphite, which is electrically conductive and quite high in its specific surface area, is an excellent gasket material for electromagnetic interference (EMI) shielding [9,11,12].

An elastomer is a material that undergoes extensive reversible mechanical deformation upon loading. A classical example of an elastomer is rubber, which deforms extensively due to the bending, straightening and segmental motions associated with the long bent molecules that make up solid rubber. Furthermore, rubber's extensive deformation is reversible, as made possible by the crosslinking between the molecules. The crosslinking process in case of rubber is known as vulcanization. The crosslinking causes covalent linkages between adjacent molecules. These linkages pull the molecules back to their original configuration upon unloading. All previously reported elastomers are amorphous polymers above their glass transition temperature, which is below room temperature in order for the material to be an elastomer at room temperature. The polymers suffer from their inability to withstand high temperatures [13] and their change from being ductile to being brittle as the temperature is lowered to below the glass transition temperature. For example, the Space Shuttle Challenger disintegrated upon reentry in 1986, due to the failure of an O-ring seal on the right solid-fuel rocket booster. The failure was partly due to the unusually low temperatures prior to lift off and the consequent brittleness of the O-ring[†]. In contrast, graphite can withstand relatively high temperatures as well as cryogenic temperatures. High temperatures are encountered in aircraft brakes, rockets, nuclear reactors, oil wells and various industrial processes. Cryogenic temperatures are encountered in applications related to cryogenic fuels for rockets, frozen food, blood banking and various industrial processes.

The enormous expansion that occurs during the exfoliation of graphite suggests that the exfoliated material may exhibit interesting mechanical properties. Indeed, it has recently been reported that exfoliated graphite exhibits a high degree of viscous character, as observed under low-amplitude cyclic loading [6,14]. A number of graphite layers (e.g., 60 [6]) are stacked to form a cell wall in the cellular structure of exfoliated graphite. The viscous character is due to the reversible dynamic low-amplitude sliding of the graphite layers relative to one another [6]. Furthermore, the viscous character decreases with increasing compaction of the worms [6], because of the decreasing ease of sliding as the degree of compaction increases. However, high-amplitude reversible sliding has not been previously reported in exfoliated graphite.

This paper is aimed at (i) observing for the first time the elastomeric behavior of exfoliated graphite, (ii) characterizing the elastomeric behavior of exfoliated graphite, (iii) determining the extents of reversible and irreversible deformation associated with the elastomeric behavior, and (iv) studying the effect of the degree of compaction on the elastomeric behavior.

The elastomeric deformation of exfoliated graphite is observed in this work by instrumented indentation testing (nanoindentation), which is conducted in the direction of compaction of the worms. Nanoindentation has been previously reported in highly oriented pyrolytic graphite [15] and amorphous carbon films [16], but it has not been previously reported in exfoliated graphite or flexible graphite.

2. Experimental methods

As in prior work [6], exfoliated graphite (worms) is obtained by rapid heating of expandable sulfuric-acid-intercalated graphite flake from Asbury (No. 3772) at 900 °C for 2 min with flowing nitrogen. The worms are of length 2–4 mm and specific surface area 41 m^2/g (measured by nitrogen adsorption using a Micromeritics ASAP 2010 instrument). The specific surface area of 41 m^2/g corresponds to about 60 graphite layers (on the average) stacked in a cell wall in the cellular structure of the exfoliated graphite. This means that the cell wall thickness is about 20 nm on the average. This cell wall thickness is consistent with the average stacking height (L_c = 24 nm) of graphite crystallites, as determined by X-ray diffraction for an exfoliated graphite compact [17]. The pressure used to compact the worms has almost no effect on L_c [17]. On the other hand, the increase in the pressure enhances the degree of preferred orientation of the graphite layers in the plane perpendicular to the direction of compaction, as shown by the increased intensity of the graphite 002 X-ray diffraction line [17].

The worms are compressed in a steel mold at pressures ranging from 1.70 to 5.25 MPa for 5 min to form exfoliated graphite compacts of density ranging from 0.089 to 0.275 g/cm^3 and carbon volume fraction (i.e., 1 – porosity) ranging from 4.01% to 12.2%. The density is determined by measurement of the mass and volume; at least four specimens are measured for each value of the fabrication pressure. The fabrication pressures used are low compared to prior work on flexible graphite [17] and are chosen in order to accentuate the viscous behavior. As a result, the density of the resulting compacts is quite low compared to commercially available flexible graphite (1.1 g/cm^3) [17]. For the sake of comparison, this work also studies commercial flexible graphite (Mineral Seal Corporation, Tucson, AZ) with density 0.86 g/cm^3 (i.e., 37.8 vol.% carbon).

Instrumented-indentation testing in the form of nanoindentation testing under load control was conducted using a nanoindenter (MTS Systems Corporation, Model XP), equipped with a diamond Berkovich indenter tip that has a triangle-pyramidal shape and an angle of 77° between the indenter axis and each of the three side faces of the indenter

[†] http://science.ksc.nasa.gov/shuttle/missions/51-l/docs/rogers-commission/Chapter-4.txt, as viewed on January 22, 2014.

tip. A high-resolution actuator is used to force the indenter into a test surface, and a high-resolution sensor is used to continuously measure the resulting penetration. The contact area under load can be inferred from the continuous load–displacement data. Thus, the residual hardness impression (the residual indent) after unloading does not have to be observed, in contrast to conventional hardness testing. The direction of indentation is that of the pressure used in forming the exfoliated graphite compact. The maximum load or the maximum displacement during indentation is selected for each test, which is under load control. The load resolution is 0.05 μN. The loading rate is 1.0 μN/s. In each loading cycle, the maximum load is held for 3 s before unloading; the displacement in this period is due to creep.

The elastic modulus E of the specimen is determined from the reduced modulus, E_r, which is obtained by using the equation[‡]

$$E_r = \frac{S\sqrt{\pi}}{2\beta\sqrt{A}}, \quad (1)$$

where S (known as the contact stiffness, i.e., the stiffness of the indenter-specimen contact) is the slope of the initial portion of the curve of load vs. displacement during unloading, β is a constant that depends only on the geometry of the indenter tip ($\beta = 1.034$ for the Berkovich tip used) and A is the projected contact area. The specimen modulus E is then obtained using the equation

$$\frac{1}{E_r} = \frac{(1-\nu^2)}{E} + \frac{(1-\nu_i^2)}{E_i}, \quad (2)$$

where E_i and ν_i are the elastic modulus and Poisson's ratio of the indenter tip ($E_i = 1141$ GPa and $\nu_i = 0.07$ for the diamond indenter tip used). The ν is the Poisson's ratio of the specimen ($\nu_{13} = 0.3$ for graphite [18]). The Continuous Stiffness Measurement (CSM) mode of operating the instrument is used. The mode allows the indenter tip to oscillate along the axis of the indentation so that S, and hence E_r and E, are obtained continuously during the testing cycle.

The area under the loading curve is the mechanical energy input during loading. The area under the unloading curve is the mechanical energy output during unloading. The mechanical energy loss in a cycle of loading is given by the hysteresis area bound by the loading and unloading load–displacement curves. This quantity tends to be higher when the irreversible displacement is larger. The fractional energy loss is defined as the energy loss divided by the energy input. This quantity tends to be higher when the fraction of displacement that is irreversible is larger.

3. Results and discussion

Table 1 and Figs. 1–4 show the nanoindentation results for exfoliated graphite compacts of various densities and for commercial flexible graphite. The smoothness of the load vs. displacement curve (i.e., the absence of discontinuities) indicates that the indentation mechanism involves the stretching of the cell walls (Fig. 5) rather than the puncturing of the walls. Puncturing would have caused one or more discontinuities in the curve, as observed in case of highly oriented pyrolytic graphite (HOPG) at a load of 1200 μN [15]. The deformation is mostly reversible upon unloading, as shown by Fig. 1 and the essential absence of an indent after unloading. In Fig. 1(a), the maximum indentation depth (770 nm) corresponds to an indent size under load of 3340 nm from the center of the indent.

The displacement is attributed to the sliding between the graphite layers in a cell wall (thickness ~20 nm), so the maximum shear strain in the cell wall is 770/~20 = ~40. This huge strain and its essential reversibility indicate elastomeric deformation, which has been previously reported in polymers only. The small degree of irreversibility after the first cycle causes the modulus to be slightly higher in the second cycle (Fig. 1(b)) – akin to strain hardening. Due to the Poisson effect, the thickness of the cell wall is expected to decrease as the shear strain occurs. Thus, the true shear strain is higher than the above value, which is actually the engineering shear strain, due to its consideration of the initial thickness rather than the instantaneous thickness of the cell wall.

The essentially reversible deformation during nanoindentation is consistent with the essential reversibility of the small-amplitude dynamic sliding between the graphite layers during vibration [6]. Though the amplitude of the sliding is small, the sliding is easy and the back-and-forth sliding during vibration provides a significant degree of viscous behavior. It is akin to the wall of a balloon stretching and recoiling at a small deformation amplitude during repeated variation in the gas pressure in the balloon.

For a fixed maximum load of 250 μN (Table 1), as the density of the exfoliated graphite increases (i.e., as the carbon volume fraction increases from 4 to 12 vol.%), the maximum displacement (1st cycle) decreases from 790 to 500 nm, the reversible displacement (1st cycle) decreases from 700 to 400 nm, the irreversible displacement (1st cycle) essentially does not change, the fraction of displacement that is reversible (1st cycle) decreases slightly from 88% to 79%, and the fraction of displacement that is irreversible (1st cycle) increases from 12% to 21%. Similarly, as the density of the exfoliated graphite compact increases, the total shear strain (1st cycle) decreases from 40 to 25 and the reversible shear strain (1st cycle) decreases from 35 to 20, whereas the irreversible shear strain (1st cycle) essentially does not change. As shown for the solid content of 4.0 vol.%, upon reloading (i.e., in the second cycle of loading), the maximum displacement and the irreversible displacement are lower than those for the first cycle, but the reversible displacement is essentially the same as that of the first cycle. Similarly, upon reloading, the total shear strain and the irreversible shear strain are lower than those of the first cycle, but the reversible shear strain is essentially the same as that of the first cycle. A strong elastomeric character is associated with a large reversible displacement. Thus, the elastomeric character diminishes with increasing density and is essentially unchanged upon reloading.

As the density of the exfoliated graphite compact increases, the initial modulus (1st cycle) increases greatly

[‡] http://www.msm.cam.ac.uk/mechtest/docs/XP%20User's%20Manual.pdf, p. 29, as viewed on January 24, 2014.

Table 1 – Nanoindentation results for various graphite materials made from exfoliated graphite. The maximum load is fixed at 250 μN. EG = exfoliated graphite.

	EG compact		EG compact[a]	EG compact[a]	Flexible graphite[a]
	1st cycle	2nd cycle			
Thickness (mm)	0.86 ± 0.03		1.01 ± 0.02	0.95 ± 0.02	3.5
Solid content (%)	4.01 ± 0.06		7.69 ± 0.11	12.2 ± 0.2	37.8
Density (g/cm^3)	0.089 ± 0.002		0.180 ± 0.003	0.275 ± 0.003	0.86
Fabrication pressure (MPa)	1.70		3.09	5.25	[b]
Maximum displacement (nm)	791 ± 49	735 ± 23	614 ± 31	502 ± 28	233 ± 11
Reversible displacement (nm)	695 ± 30	681 ± 19	523 ± 25	398 ± 17	166 ± 7
Irreversible displacement (nm)	95.9 ± 7.3	54.1 ± 3.0	91.4 ± 4.9	104 ± 8	67.3 ± 4.4
Fraction of displacement that is reversible (%)	87.9 ± 3.4	92.5 ± 1.2	85.2 ± 1.9	79.3 ± 2.5	71.2 ± 1.7
Fraction of displacement that is irreversible (%)	12.1 ± 1.3	7.46 ± 0.34	14.8 ± 0.6	20.7 ± 1.1	28.8 ± 0.9
Total shear strain	39.6 ± 2.5	36.8 ± 1.2	30.7 ± 1.6	25.1 ± 1.4	11.7 ± 0.6
Reversible shear strain	34.8 ± 1.5	34.1 ± 1.0	26.2 ± 1.3	19.9 ± 0.9	8.3 ± 0.4
Irreversible shear strain	4.8 ± 0.4	2.7 ± 0.2	4.6 ± 0.3	5.2 ± 0.4	3.4 ± 0.2
Initial modulus (kPa)	83 ± 6	115 ± 4	164 ± 4	191 ± 6	792 ± 19
Modulus at maximum displacement (kPa)	125 ± 11	165 ± 5	213 ± 6	251 ± 6	1071 ± 28
Load per unit displacement (μN/nm)	0.32 ± 0.02	0.34 ± 0.01	0.41 ± 0.02	0.50 ± 0.03	1.07 ± 0.04
Energy loss (10^{-11} J)	1.01 ± 0.15	0.66 ± 0.03	1.19 ± 0.04	1.03 ± 0.03	0.73 ± 0.06
Fractional energy loss (%)	11.9 ± 0.9	7.3 ± 0.8	13.2 ± 0.6	16.8 ± 0.4	23.9 ± 1.1

[a] 1st cycle.
[b] Proprietary to the manufacturer of the flexible graphite.

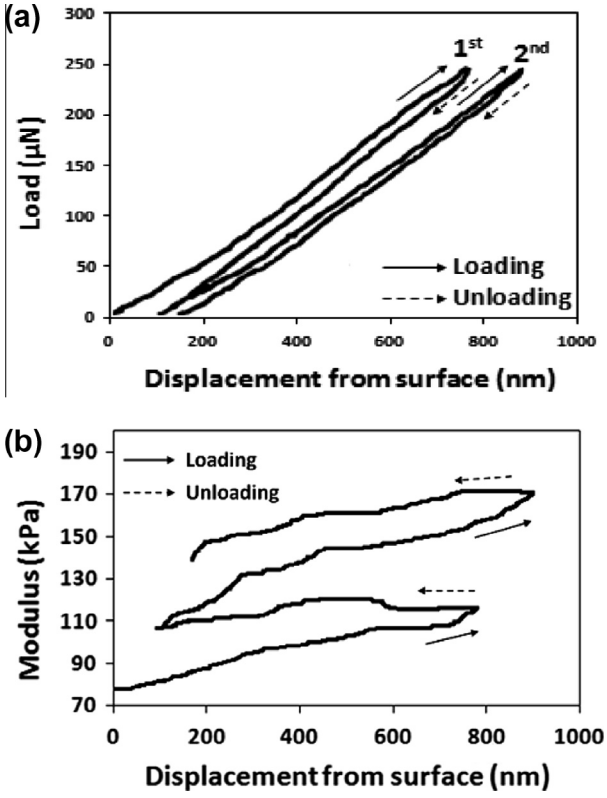

Fig. 1 – Nanoindentation results obtained during the first two cycles of loading of an exfoliated graphite compact with 4.01 vol.% solid. (a) Curve of load vs. displacement. (b) Curve of modulus vs. displacement.

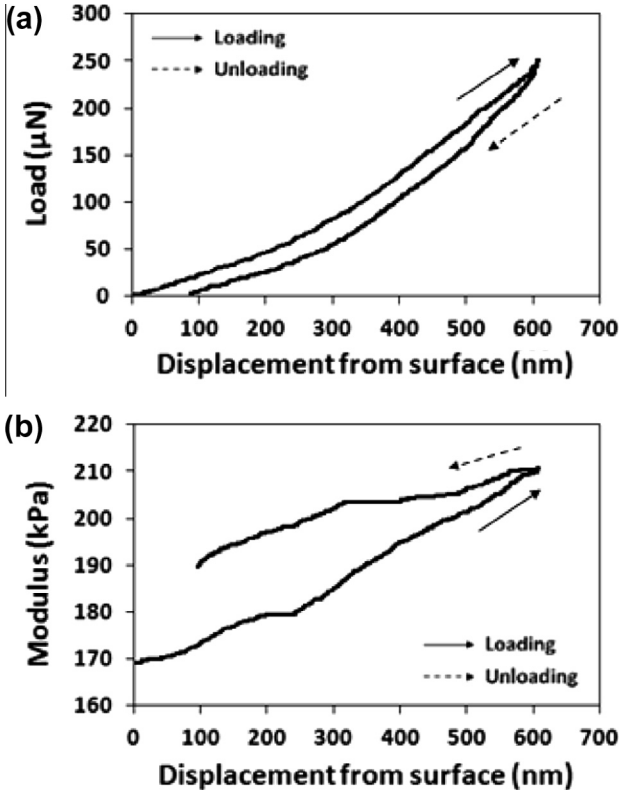

Fig. 2 – Nanoindentation results obtained during the first cycle of loading of an exfoliated graphite compact with 7.69 vol.% solid. (a) Curve of load vs. displacement. (b) Curve of modulus vs. displacement.

from 83 to 191 kPa and the modulus at the maximum displacement (1st cycle) increases substantially from 125 to 251 kPa. As shown for the solid content of 4.0 vol.%, upon reloading (i.e., in the second cycle of loading), both the initial modulus and the modulus at the maximum displacement increase substantially. This means that the exfoliated graphite com-

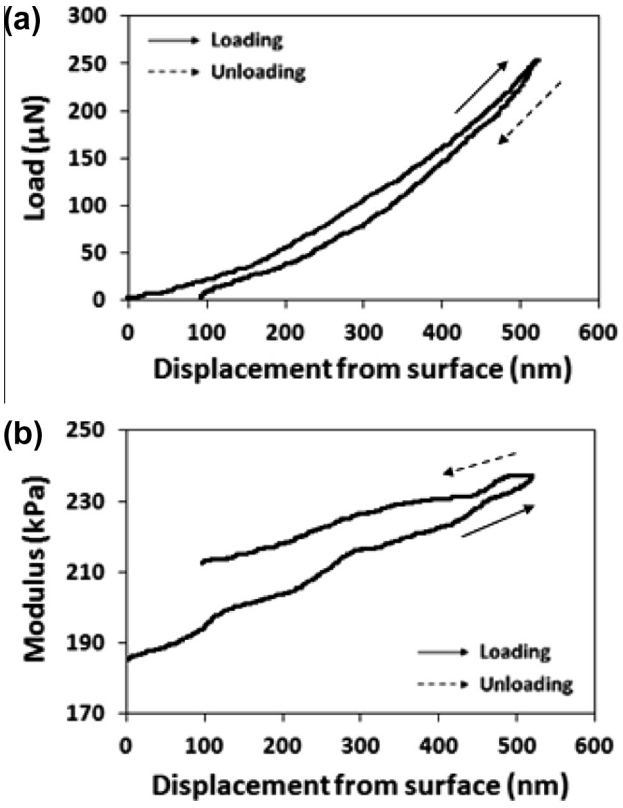

Fig. 3 – Nanoindentation results obtained during the first cycle of loading of an exfoliated graphite compact with 12.2 vol.% solid. (a) Curve of load vs. displacement. (b) Curve of modulus vs. displacement.

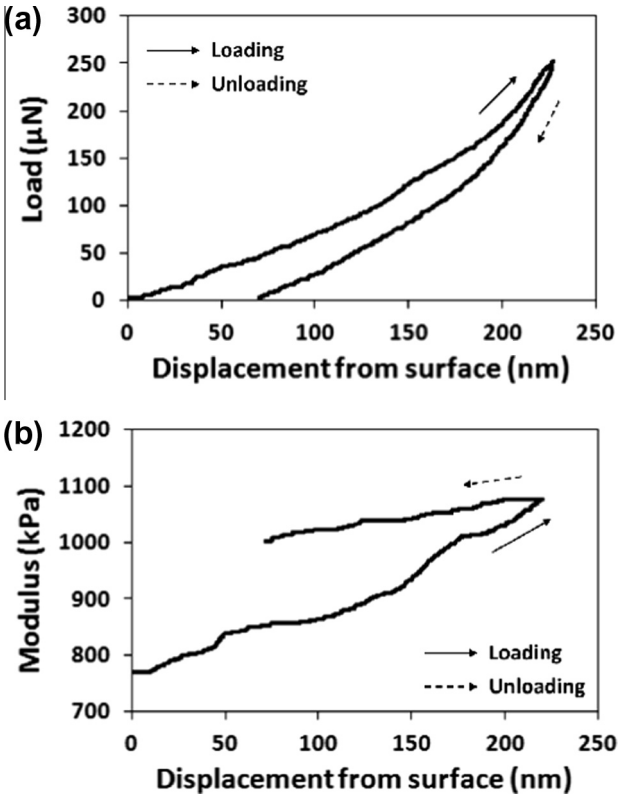

Fig. 4 – Nanoindentation results obtained during the first cycle of loading of commercial flexible graphite. (a) Curve of load vs. displacement. (b) Curve of modulus vs. displacement.

pact becomes stiffer as the density increases and upon reloading. The stiffening upon density increase is consistent with the decrease in the elastomeric character. However, in spite of the stiffening upon reloading, the elastomeric character is not changed upon reloading.

The load per unit displacement (1st cycle) during nanoindentation of the exfoliated graphite compact increases from 0.32 to 0.50 μN/nm as the density increases. This is consistent with the increase in modulus, the increase in the fraction of displacement that is irreversible, and the decrease in the maximum displacement as the density increases. This means that a high degree of compaction of exfoliated graphite causes the deformation during indentation to be less reversible and the modulus to be higher. In other words, a high degree of compaction makes the sliding between the graphite layers more difficult, with presumably more irreversible microstructural change incurred during the sliding. This is consistent with a decrease in the loss tangent and an increase in the storage modulus of an exfoliated graphite compact under dynamic flexure or under dynamic compression at low amplitudes in the compaction direction, as the degree of compaction increases [6]. The abovementioned effects of the degree of compaction on the nanoindentation results may also be due to the increase in the preferred orientation of the graphite layers in the plane perpendicular to the compaction direction as the degree of compaction increases [17] and the consequent decrease in the average resolved shear stress parallel to the graphite layers during indentation as the degree of compaction increases.

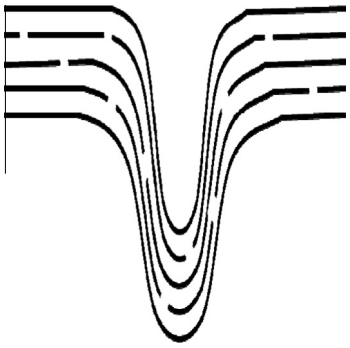

Fig. 5 – Schematic illustration of a cell wall that has been extended by indentation from the top, thereby forming an indent with almost complete reversibility upon unloading. The highest reversible deformation observed in this work is much greater than what this drawing depicts.

For flexible graphite, which has a higher density than any of the exfoliated graphite compacts, the load per unit displacement is even higher, namely 1.1 μN/nm. This is consistent with the high modulus, the low displacement and the low shear strain of flexible graphite compared to any of the exfoliated graphite compacts. Furthermore, the fraction of displa-

cement that is irreversible is higher for flexible graphite than any of the exfoliated graphite compacts.

The energy loss in the first cycle is higher for any of the exfoliated graphite compacts than flexible graphite. This reflects the greater irreversible displacement for the compacts than flexible graphite. The energy loss is considerably lower for the second cycle than the first cycle, due to the lower irreversible displacement in the second cycle. The fractional energy loss is lower for any of the exfoliated graphite compacts than flexible graphite, because of the smaller fraction of displacement that is irreversible for the compacts. The fractional energy loss increases with increasing solid content. For the same solid content, it is lower for the second cycle than the first cycle.

From a scientific viewpoint, comparison at a fixed maximum displacement is more meaningful than comparison at a fixed maximum load. Table 2 shows the effect of the solid content for a fixed maximum displacement of 500 nm. The reversible displacement, fractional of displacement that is reversible and the reversible shear strain all decrease with increasing solid content. In contrast, the irreversible displacement, the fraction of displacement that is irreversible and the irreversible shear strain all increase with increasing solid content. This means that the strain reversibility decreases with increasing solid content. The initial modulus, the modulus at maximum displacement and the load per unit displacement all increase with increasing solid content, indicating that the stiffness increases with increasing solid content, as expected.

Table 3 and Fig. 6 show that, at a fixed solid content of 4.0 vol.%, increase in the maximum load increases the maximum displacement, such that the load per unit displacement is essentially not affected. Moreover, increase in the maximum load increases the modulus at the maximum displacement, but it has no effect on the initial modulus. In addition, increase in the maximum load causes the reversible displacement and the irreversible displacement to increase, such that the fraction of displacement that is reversible and the fraction of displacement that is irreversible are essentially not affected. Increase in the maximum load causes the total shear strain, the reversible shear strain and the irreversible shear strain to increase, such that the irreversible shear strain is much smaller than the reversible shear strain for any of the maximum loads. Hence, similar elastomeric character is observed for various maximum loads.

Table 4 and Fig. 7 show a comparison of the results for the flexible graphite (the same as the commercial flexible graphite in Table 1) tested at different values of the maximum displacement. The total shear strain, the reversible shear strain and the irreversible shear strain all increase with increasing maximum displacement. The fraction of displacement that is reversible decreases with increasing maximum displacement, whereas the fraction of displacement that is irreversible increases with increasing displacement. The trends for all these quantities are the same as those for exfoliated graphite (Table 3). For a similar maximum displacement of around 500 nm (500 nm in Table 4 and 524 nm in Table 3), comparison of Tables 3 and 4 shows that the total shear strain is similar (26 and 25 for Tables 3 and 4 respectively), but the reversible shear strain is higher for Table 3 (23) than Table 4 (17) and the irreversible shear strain is lower for Table 3 (2.8) than Table 4 (8.4). Similarly, for a similar maximum displacement of around 750 nm (750 nm in Table 4 and 790 nm in Table 3), comparison of Tables 3 and 4 show that the total shear strain is similar (40 and 38 for Tables 3 and 4 respectively), but the reversible shear strain is higher for Table 3 (35) than Table 4 (24) and the irreversible shear strain is lower for Table 3 (5) than Table 4 (13). This means that, at similar values of the maximum displacement, the exfoliated graphite compact (4 vol.% solid) and the flexible graphite (38 vol.% solid) give similar values of the total shear strain, but the strain is more reversible for the exfoliated graphite compact than the flexible graphite. The greater degree of strain reversibility for the exfoliated graphite compact compared to flexible graphite is also indicated by comparison of Figs. 6 and 7. To reach a similar value of the maximum displacement, flexible graphite requires much higher maximum load than the exfoliated graphite, as expected and as shown by comparing Tables 3 and 4.

The load needed per unit penetration during nanoindentation is 6.0 and 13 μN/nm for HOPG [15] and amorphous carbon film [16] respectively. These values are much higher than those for flexible graphite or any of the exfoliated graphite compacts (Table 1). In spite of HOPG's very high degree of preferred orientation of the graphite layers in the plane of the material and the softness of graphite along the c-axis, HOPG

Table 2 – Nanoindentation results for exfoliated graphite compacts at three different solid contents. The maximum displacement was fixed at 500 nm. All data are for the first cycle.

Solid content (vol.%)	4.01 ± 0.06	7.69 ± 0.11	12.2 ± 0.2
Maximum load (μN)	163 ± 6	175 ± 6	248 ± 9
Reversible displacement (nm)	451 ± 20	421 ± 18	391 ± 15
Irreversible displacement (nm)	49.1 ± 3.8	79.4 ± 4.3	108 ± 8
Fraction of displacement that is reversible (%)	90.3 ± 2.4	84.3 ± 2.9	78.2 ± 2.3
Fraction of displacement that is irreversible (%)	9.7 ± 1.1	15.7 ± 1.5	21.8 ± 1.5
Total shear strain	25	25	25
Reversible shear strain	22.6 ± 1.0	21.1 ± 0.9	19.6 ± 0.8
Irreversible shear strain	2.5 ± 0.2	4.0 ± 0.2	5.4 ± 0.4
Initial modulus (kPa)	74 ± 9	161 ± 6	189 ± 4
Modulus at maximum displacement (kPa)	109 ± 12	189 ± 11	241 ± 7
Load per unit displacement (μN/nm)	0.33 ± 0.02	0.35 ± 0.03	0.50 ± 0.03

Table 3 – Nanoindentation results for exfoliated graphite compacts at a fixed solid content of 4.01 ± 0.06 vol.%. The maximum load is varied. All data are for the first cycle.

Maximum load (μN)	100	175	250
Maximum displacement (nm)	288 ± 19	524 ± 27	791 ± 49
Reversible displacement (nm)	260 ± 17	468 ± 22	695 ± 30
Irreversible displacement (nm)	28.4 ± 1.3	56.1 ± 3.3	95.9 ± 7.3
Fraction of displacement that is reversible (%)	90.3 ± 2.9	89.3 ± 3.3	87.9 ± 3.4
Fraction of displacement that is irreversible (%)	9.72 ± 0.77	10.7 ± 1.0	12.1 ± 1.3
Total shear strain	14.4 ± 1.1	26.2 ± 1.4	39.6 ± 2.5
Reversible shear strain	13.0 ± 0.9	23.4 ± 1.1	34.8 ± 1.5
Irreversible shear strain	1.42 ± 0.07	2.8 ± 0.2	4.8 ± 0.4
Initial modulus (kPa)	72 ± 5	79 ± 6	83 ± 6
Modulus at maximum displacement (kPa)	74 ± 7	89 ± 10	125 ± 11
Load per unit displacement (μN/nm)	0.34 ± 0.03	0.34 ± 0.02	0.32 ± 0.02

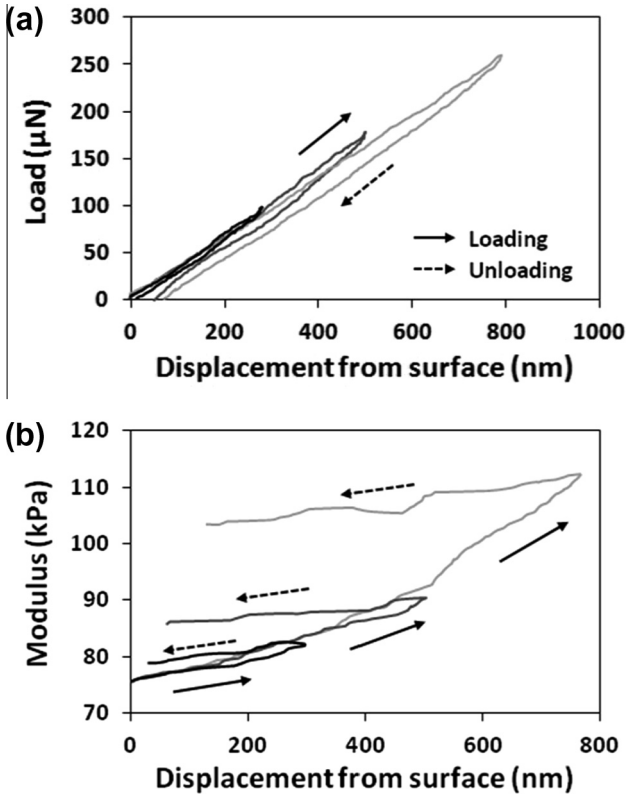

Fig. 6 – Nanoindentation results for exfoliated graphite compacts at a fixed solid content of 4.01 ± 0.06 vol.%. The maximum load is varied. All curves are for the first cycle. Solid arrow: loading. Dashed arrow: unloading.

is much stiffer than both exfoliated graphite and flexible graphite. This suggests that the cell wall present in both exfoliated graphite and flexible graphite enables greater ease of sliding between the graphite layers than HOPG. The exfoliation process causes loosening of the layers relative to one another. HOPG has not undergone this loosening. Due to its amorphous structure, the amorphous carbon film resists sliding and hence results in even greater resistance to nanoindentation than HOPG.

The elastomeric behavior is due to the high strain made possible by the sliding of the graphite layers within a cell wall of exfoliated graphite. The reversibility of the sliding is probably made possible by the ease of sliding of the graphite layers and the cellular structure, in which the extremities (corners) of a cell serve as pinning points that effectively link the graphite layers (Fig. 8). The ability of rubber to exhibit reversible strain is due to the crosslinks. The pinning points in exfoliated graphite are probably akin to the crosslinks in rubber.

The evidence for the elastomeric behavior is not only based on the reversibility of the indentation deformation. The mechanism of the deformation involves the shear deformation of the cell wall of exfoliated graphite. With the thickness of about 20 nm for the cell wall, the deformation observed by instrumented indentation corresponds to a shear strain of up to 40 in the cell wall. This huge shear strain and its essential reversibility support the description of the deformation as being elastomeric. For rubbers, which are well-known polymeric elastomers, the ductility ranges from 1 to 9 (http://www-materials.eng.cam.ac.uk/mpsite/properties/non-IE/elongation.html, as viewed on September 19, 2014). Hence, the strain of up to 40 observed in the cell wall exceeds the strain capacity of rubbers.

Prior work involving instrumented indentation of glassy carbon, pyrolytic graphite and heat-treated carbons shows also a strong degree of reversibility in the deformation [19–21]. However, the deformation differs greatly from that of the exfoliated graphite compacts of this work in both the deformation characteristics and the deformation mechanism. In particular, the load per unit displacement is much higher for the carbons of the prior work than the exfoliated graphite compacts. For example, the load per unit displacement is 700 and 270 μN/nm for carbons heat treated at 880 and 2600 °C respectively [19], 100 μN/nm for glassy carbon [21] and 16 μN/nm for pyrolytic graphite [21]. In contrast the load per unit displacement ranges from 0.3 to 0.5 μN/nm for the exfoliated graphite compacts of this work. In addition, the modulus of the carbons in the prior work is much higher than that of the exfoliated graphite compacts. For example, the modulus is 19.2 and 10.8 GPa for the carbons heat-treated at 880 and 2600 °C respectively, whereas it ranges from 110 to 250 kPa for the exfoliated graphite compacts. This means that the exfoliated graphite compacts are much more deformable than the carbons of the prior work. This large difference in deformation characteristics between the prior work and this

Table 4 – Nanoindentation results for flexible graphite (same as the flexible graphite in Table 1). The maximum displacement/load is varied. All data are for the first cycle.

Maximum load (μN)	250[a]	581 ± 22	1072 ± 45	1882 ± 77
Maximum displacement (nm)	233 ± 11	500[b]	750[b]	1000[b]
Reversible displacement (nm)	166 ± 7	333 ± 13	487 ± 20	603 ± 38
Irreversible displacement (nm)	67.3 ± 4.4	167 ± 9	263 ± 16	397 ± 29
Fraction of displacement that is reversible (%)	71.2 ± 1.7	66.6 ± 2.0	64.9 ± 2.3	60.3 ± 1.4
Fraction of displacement that is irreversible (%)	28.8 ± 0.9	33.4 ± 1.1	35.1 ± 1.3	39.7 ± 0.8
Total shear strain	11.7 ± 0.6	25	37.5	50
Reversible shear strain	8.3 ± 0.4	16.7 ± 0.7	24.4 ± 1.0	30.2 ± 1.9
Irreversible shear strain	3.4 ± 0.2	8.4 ± 0.5	13.1 ± 0.8	19.8 ± 1.5
Modulus at maximum displacement (kPa)	1071 ± 28	1244 ± 35	1556 ± 59	1698 ± 83
Load per unit displacement (μN/nm)	1.07 ± 0.04	1.16 ± 0.05	1.43 ± 0.06	1.88 ± 0.07

[a] Maximum load being set at the value indicated.
[b] Maximum displacement being set at the value indicated.

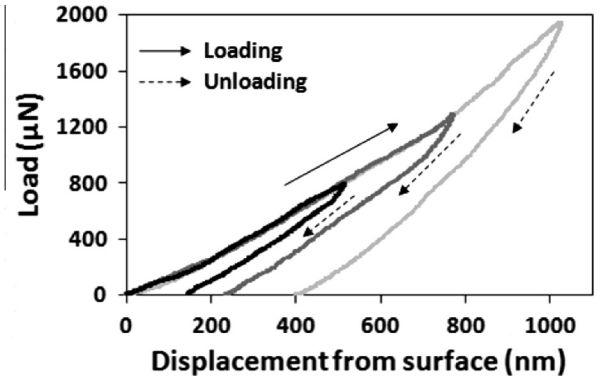

Fig. 7 – Nanoindentation results for flexible graphite. The maximum displacement is varied. All curves are for the first cycle.

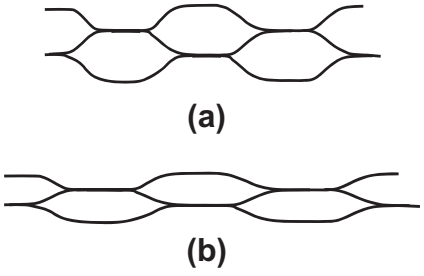

Fig. 8 – Schematic illustration (not to scale) of the cellular structure of exfoliated graphite. The cell wall, which is a nanoscale multilayer that consists of about 60 graphite layers, can stretch greatly due to the sliding of the graphite layers with respect to one another. The solid line denotes the cell wall. The individual layers in the multilayer are not shown. (a) Before loading. (b) During loading.

work is due to the difference in deformation mechanism. In the prior work, the mechanism involves elastoplastic deformation, such that the reversibility of the plastic part of the deformation is believed to be due to reversible slip of the dislocation-network structures on the graphitic basal planes [19]. Due to the high modulus and consequent low deformability of the carbons of the prior work, the deformation in the prior work is not considered elastomeric, in spite of its reversibility. In contrast, the mechanism of the deformation in the exfoliated graphite compacts is associated with the sliding of the graphite layers within the cell wall of exfoliated graphite. This sliding, as illustrated in Fig. 5, enables the huge shear strain in the cell wall during indentation. Nevertheless, the elastomeric deformation can be considered a type of elastoplastic deformation. The elastomeric character is consistent with the well-known resiliency of flexible graphite in the through-thickness direction. This resiliency enables flexible graphite to be used as a gasket material. Such resiliency is absent in the carbons of the prior work (which are not used as gasket materials), in spite of the reversibility of their indentation deformation.

The deformation in flexible graphite (Fig. 4) is less reversible than that in the exfoliated graphite compacts (Figs. 1–3) and is also less reversible than that in the carbons of the prior work [19–21]. This difference between flexible graphite and the carbons of the prior work occurs in spite of the low modulus (ranging from 1100 to 1700 kPa) and low load per unit displacement (ranging from 1.1 to 1.9 μN/nm) of flexible graphite and the much higher values (mentioned above) for the carbons of the prior work. This difference again points to the difference in deformation mechanism. Probably due to greater friction in the sliding of the graphite layers in the cell wall in flexible graphite compared to that in the exfoliated graphite compacts, the deformation is less reversible for flexible graphite than the exfoliated graphite compacts. In spite of the high deformability of flexible graphite compared to the carbons of the prior work, the relatively low reversibility of the deformation of flexible graphite makes the deformation not considered elastomeric.

4. Conclusion

This paper reports for the first time the elastomeric behavior of a non-polymeric material. The observation is made in exfoliated graphite compacts (⩽12 vol.% solid, preferably 4 vol.% solid) and is enabled by the high-amplitude reversible and easy sliding of the graphite layers relative to one another in the cell wall (~60 graphite layers) of exfoliated graphite. Similar elastomeric character occurs for various maximum loads. The elastomeric behavior is consistent with the interface-

derived extraordinary viscous behavior of exfoliated graphite [14].

The reversibility of the deformation is probably enabled by the pinning of the graphite layers at the extremities of each cell. The nanoindentation deformation mechanism involves the stretching of the cell walls rather than the puncturing of the walls. The deformation is mostly reversible upon unloading. The elastomeric character diminishes with increasing degree of compaction and is essentially unchanged upon reloading. The small degree of irreversibility after the first cycle causes the modulus to be higher in the second cycle.

The total engineering shear strain and reversible engineering shear strain of the cell wall are up to 40 and 35 respectively during nanoindentation (in the compaction direction) without fracture of the graphite layers, compared to corresponding values of 12 and 8 for flexible graphite with 38 vol.% solid. The fraction of displacement that is irreversible is as low as 12%, compared to 29% for flexible graphite. The fractional energy loss is as low as 12%, compared to 24% for flexible graphite. The modulus is as low as 83 kPa, compared to 790 kPa for flexible graphite. The load per unit displacement is as low as 0.32 μN/nm, compared to 1.1 μN/nm for flexible graphite. The greater the degree of compaction, the lower are the shear strain and the deformation reversibility, and the higher are the modulus and the load needed for displacement. For the same maximum displacement, the total strain in an exfoliated graphite compact is similar to that for the flexible graphite, but the strain is more reversible for the former.

HOPG of prior work [15] experiences graphite layer fracture upon indentation at a sufficient load, and requires a relatively high load per unit displacement. The ease of sliding between graphite layers is inadequate in both flexible graphite and highly oriented pyrolytic graphite for substantial elastomeric behavior. In contrast, the ease of sliding between the graphite layers in the cell wall of exfoliated graphite is adequate for elastomeric behavior, particularly when the degree of compaction of the exfoliated graphite is low.

Acknowledgement

The authors are grateful to Professor Cemalettin Basaran of University at Buffalo, State University of New York, for the use of his nanoindenter.

REFERENCES

[1] Chung DDL. Exfoliation of graphite. J Mater Sci 1987;22(12):4190–8.
[2] Chung DDL. Graphite. J Mater Sci 2002;37(8):1475–89.
[3] Inagaki M, Kang F, Toyoda M. Exfoliation of graphite via intercalation compounds. Chem Phys Carbon 2004;29:1–69.
[4] Daumas N, Herold A. Relations between phase concept and reaction mechanics in graphite insertion compounds. CR Hebd Acad Sci C 1969;268:373–82.
[5] Anderson SH, Chung DDL. Exfoliation of intercalated graphite. Carbon 1984;22(3):253–63.
[6] Chen P, Chung DDL. Viscoelastic behavior of the cell wall of exfoliated graphite. Carbon 2013;61:305–12.
[7] Ionov SG, Avdeev VV, Kuvshinnikov SV, Pavlova EP. Physical and chemical properties of flexible graphite foils. Mol Cryst Liq Cryst Sci Technol, Sect A 2000;340:349–54.
[8] Chung DDL. Flexible graphite for gasketing, adsorption, electromagnetic interference shielding, vibration damping, electrochemical applications, and stress sensing. J Mater Eng Perform 2000;9(2):161–3.
[9] Luo X, Chung DDL. Electromagnetic interference shielding reaching 130 dB using flexible graphite. Carbon 1996;34(10):1293–4.
[10] Nassar SA, Alkelani AA. Clamp load loss due to elastic interaction and gasket creep relaxation in bolted joints. J Pressure Vessel Technol 2006;128(3):394–401.
[11] Chung DDL. Electromagnetic interference shielding effectiveness of carbon materials. Carbon 2001;39(2):279–85.
[12] Luo X, Chugh R, Biller BC, Hoi YM, Chung DDL. Electronic applications of flexible graphite. J Electron Mater 2002;31(5):535–44.
[13] Tao Z, Viriyabanthorn N, Ghumman B, Barry C, Mead J. Heat resistant elastomers. Rubber Chem Technol 2005;78(3):489–515.
[14] Chung DDL. Interface-derived extraordinary viscous behavior of exfoliated graphite. Carbon 2014;68:646–52.
[15] Richter A, Ries R, Smith R, Henkel M, Wolf B. Nanoindentation of diamond, graphite and fullerene films. Diam Relat Mater 2000;9(2):170–84.
[16] Fan X, Nose K, Diao D, Yoshida T. Nanoindentation behaviors of amorphous carbon films containing nanocrystalline graphite and diamond clusters prepared by radio frequency sputtering. Appl Surf Sci 2013;273:816–23.
[17] Wei XH, Liu L, Zhang JX, Shi JL, Guo QG. Mechanical, electrical, thermal performances and structure characteristics of flexible graphite sheets. J Mater Sci 2010;45:2449–55.
[18] Kelly BT. Physics of graphite. London: Applied Science Publishers; 1981. p. 43–4.
[19] Sakai M, Nakano Y, Shimizu S. Elastoplastic indentation on heat-treated carbons. J Am Ceram Soc 2002;85(6):1522–8.
[20] Iwashita N, Swain MV, Field JS, Ohta N, Bitoh S. Elasto-plastic deformation of glass-like carbons heat-treated at different temperatures. Carbon 2001;39:1525–32.
[21] Field JS, Swain MV. The indentation characterisation of the mechanical properties of various carbon materials: glassy carbon, coke and pyrolytic graphite. Carbon 1996;34(11):1357–66.